Article

Design, Modelling and Simulation of a Wing Sail Land Yacht

Vítor Tinoco[1], **Benedita Malheiro** [1,2*] and **Manuel F. Silva** [1,2]

1 ISEP/IPP – School of Engineering, Polytechnic of Porto, Porto, Portugal; {1141231,mbm,mss}@isep.ipp.pt
2 INESC TEC, Porto, Portugal;
* Correspondence: mbm@isep.ipp.pt

Version March 17, 2021 submitted to Appl. Sci.

Featured Application: This work describes the design, modelling and simulation of a free-rotating wing sail solution for an autonomous environmental land yacht probe. The adopted method involves the application of land sailing principles for the design, the usage of Fusion 360 tool for 3D modelling and the integration of Gazebo with the Robotic Operating System (ROS) framework for the simulation of the land yacht.

Abstract: Autonomous land yachts can play a major role in the context of environmental monitoring, namely, in open, flat, windy regions such as iced planes or sandy shorelines. This work addresses the design, modelling and simulation of a land yacht probe equipped with a rigid free-rotating wing sail and tail flap. The wing was designed with a symmetrical airfoil and dimensions to provide the necessary thrust to displace the vehicle. Specifically, it proposes a novel design and simulation method for free rotating wing sail autonomous land yachts. The simulation relies on the Gazebo simulator together with the ROS middleware. It uses a modified Gazebo aerodynamics plugin to generate the lift and drag forces and the yawing moment, two newly created plugins, one to act as a wind sensor and the other to set the wing flap angular position, and the 3D model of the land yacht created with Fusion 360. The wing sail aligns automatically to the wind direction and can be set to any given angle of attack, stabilising after a few seconds. Finally, the obtained polar diagram characterises the expected sailing performance of the land yacht. The described method can be adopted to evaluate different wing sail configurations as well as control techniques for autonomous land yachts.

Keywords: Robotic sailing; design; modelling; simulation; wing sail; flap tail; land yacht

1. Introduction

In the last decades a broad range of research has been conducted in autonomous systems, ranging from land to marine or aerial robots, since these vehicles are useful in a very broad spectrum of tasks, due to their ability to remove humans from dangerous environments, relieve them of tedious tasks, or simply go to locations otherwise inaccessible or inhospitable [1]. Diverse applications have been envisaged for these platforms, from exploration of remote places [2] to warfare [3].

In order to have truly autonomous systems, they must present not only control autonomy, but also energy autonomy. A possibility for granting energy autonomy to land and marine vehicles is to make use of wind to propel the vehicle [4] and, eventually, to power its on-board systems [5–7]. To propel these vehicles, can be adopted "traditional" cloth sails (the most common approach), rigid wing sails and mechanical devices, such as Flettner rotors and vertical and horizontal axis turbines or, even, more uncommon options, such as different sail concepts or towing kites [8].

Sailing with conventional cloth sails has been practised all around the world for thousands of years and virtually all boats, apart from those in recent sailing history, used conventional fabric sails [4].

Although flexible fabric sails have a number of useful properties, especially when controlled by a human sailor, they also present a number of limitations and / or drawbacks which can be overcome by alternative sail types, in particular rigid wing sails [8]. Among the advantages of using rigid wing sails for autonomous systems are the fact that its control is easier to automate and their increased reliability [8]. Given these advantages, the use of rigid wing sails has been proposed, for example, for powering commercial ships [9].

The vast majority of robotic sailing research is focused on wind propelled water platforms – sailboats; however, there is a lesser common type of sailing vehicles – land yachts. As autonomous robotic platforms, land yachts can play an important role in the context of environmental monitoring, namely, in the case of open flat windy regions, such as iced planes or sandy shorelines. As a result, autonomous land yachts can be used to monitor river, lake or ocean shoreline environments, or even for planetary exploration [10]. Like a sailboat, a land yacht does not require motors for propulsion, as it uses the wind, resulting in a considerable increase in power autonomy [11–13].

Although the majority of the autonomous sailing research addresses sailboats, there are also works on land yachts. The latter include the contributions of:

1. Landis *et al.* [10,14] propose the NASA Zephyr land sailing rover. It is intended to be used in Venus, a harsh, windy planet. The conceptual design uses a NACA0015 airfoil with a wingspan of 5.44 m, a lateral area of 12 m^2 and weighs 49 kg. The chassis has a triangular shape with three wheels and weighs 35 kg.
2. Xie *et al.* [11] present the Autonomous Controlled Four Wheeled Land Yacht concept. This land vehicle is propelled by a single wing sail with a symmetrical profile, 1 m wingspan, a lateral area of 0.25 m^2, a mass of 2.15 kg and a rotation range of 0° to 360°. The chassis is composed by an aluminium hull and two front and two rear wheels with a total mass of 19 kg.
3. Chen *et al.* [15] propose the Multiple Wing Sail Land Yacht. It adopts a triple wing sail design to reduce the wind velocity required to start the vehicle motion. The remaining features are equal to those of the previous example.
4. Zhu *et al.* [13] adopt a free-rotating NACA0015 wing sail with a wingspan of 2.5 m and a lateral area of 1.25 m^2 design to rig a land yacht. The steel chassis has one front wheel and two rear wheels. Although not fully autonomous, the angle of attack of the free-rotating wing sail is set by controlling the tail flap, which induces torque on the wing sail.
5. Mirzaei *et al.* [16] describe a land yacht developed with a NACA0012 airfoil. The airfoil has a wingspan of 1 m and a lateral area of 0.5 m^2. The chassis has a triangular shape with a front wheel and two rear wheels and has a mass of 8 kg.
6. Dong *et al.* [17] describe a land yacht with a wing sail and a chassis. The NACA0015 airfoil has a wingspan of 0.8 m, a lateral area of 0.24 m^2 and a rotation range of 0° to 270°. The chassis has four steel wheels and plastic frame.
7. Reina *et al.* [18] detail a land yacht model which has a NACA0012 airfoil with a wingspan of 3 m and a lateral area of 2 m^2. The triangular chassis has three wheels and weighs 100 kg.

The main characteristics of the above reviewed land yachts are compared in Table 1. All these prototypes share the type of sail – symmetrical wing sails – and perception sensors – Global Navigation Satellite Systems (GNSS) receivers, inertial and wind direction and velocity units. Apart from the proposals of [13,17,18], the remaining platforms adopt a four wheeled chassis with a higher rear wheel baseline. This design option provides, according to [11,15,16], greater stability and maneuverability.

Land yachts are not only governed by the principles of sailing [4], but sail design is an essential part of their development [19]. The research and development performed on rigid-wing sails has a much bigger scope than just land yachts. This type of sails is, as previously stated, commonly used in marine vessels such as sailboats. Like the autonomous land yachts, several autonomous rigid-wing sailboats have been developed by the scientific community. Some examples of these vessels are: (*i*) the Atlantis autonomous catamaran [20] which uses a NACA0015 airfoil as the wing sail with a wingspan of 5.37 m and a lateral area of 7.8 m^2. Furthermore, the wing sail is free rotating, meaning it is not

Table 1. Reviewed Autonomous Land Yachts

Source	Wing Sail						Chassis		
	Airfoil	Free Rot.	Angle Range (°)	Wingspan (m)	Lat. Area (m^2)	Mass (kg)	Material	Wheels	Mass (kg)
Xie *et al.* [11]	NACA0018	No	0 to 360	1	0.25	2.15	Aluminum	4	19
Chen *et al.* [15]	3 x NACA0018	No	0 to 360	3 x 1	3 x 0.25	3 x 2.15	Aluminum	4	19
Zhu *et al.* [13]	NACA0015	Yes	0 to 360	2.5	1.25	-	Steel	4	-
Mirzaei *et al.* [16]	NACA0012	No	-	1	0.5	-	-	3	8
Dong *et al.* [17]	NACA0015	No	0 to 270	0.8	0.24	-	Steel & Plastic	4	-
Reina *et al.* [18]	NACA0012	No	-	3	0.66	-	-	3	100
Geoffrey *et al.* [10]	NACA0015	No	-	5.44	12	49	-	3	35

controlled directly and aligns with the wind direction (as it is a symmetrical airfoil). Instead, the wing sail is controlled by a wing flap that induces torque on the wing sail, making it shift slightly to an angle of attack; *(ii)* the AROO sailboat [21] which uses a rigid-wing sail with a wingspan of 1.30 m and a lateral area of 0.23 m^2; (*iii*) the ASPire [22], which uses a free-rotating wing sail with a NACA63_2-618 profile. The wing sail wingspan is of 2.8 m and the lateral area is of 2.1 m^2. The focus of this work is on a land vehicle; however, as mentioned before, the research performed on marine vessels can be used on a land yacht, namely the wing sail.

Considering the modelling and/or simulation of platforms propelled by wing sails, there is scant research on land yachts:

1. Chen *et al.* [23] derive a mathematical model for a four-wheel land yacht powered by a wing sail. They model the structure, steering gear, servomotors and force of wing sail and, then, simulate the motion of land yacht according to the mathematical model. The mathematical model analyzes both the linear and steering motions. The simulation and actual experimental results confirm the feasibility and reliability of the proposed land-yacht modeling.
2. Dong *et al.* [17] present the design, simulation and development of a wind-driven land yacht propelled by a wing sail. The authors conduct a theoretical analysis and use the ANSYS Fluent simulation software to determine the lift and drag coefficients corresponding to each combination of attack and heading angles, and the best attack angle corresponding to each different heading angle. The simulation and experimental upwind results were concordant.

The modelling and/or simulation of sailboat platforms equipped with wing sails is more abundant. The following list holds a set of representative works:

1. Rynne and von Ellenrieder [24] design, simulate and develop a wind (rigid wing sail) and solar-powered autonomous surface vehicle (ASV). Before building the ASV, the control simulation was performed with a velocity prediction program (VPP). Initial field trials showed that the experimental and simulated boat speeds and wind speed/directions were consistent.
2. Enqvist *et al.* [25] design and simulate a simple, reliable and highly autonomous sailboat. They choose a symmetrical, free-rotating wing sail with an additional tail for actuating the wing and controlling its angle of attack. The design was further investigated with a computation flow dynamics simulation software.
3. Augenstein *et al.* [26] design and simulate small (1 m) semi-autonomous robotic sailboat platform variants equipped with a symmetric airfoil sail, a thin, bulbed keel, and a tail-vane rudder, replacing the traditional water rudder. They adopt MATLAB to perform 2D and 3D dynamic simulations of the tail-vane rudder design.
4. Setiawan *et al.* [27] design and simulate an autonomous sailboat dynamic model with four degrees of freedom. The simulations were carried out with MATLAB/Simulink to determine the effect of flap and rudder deflection angles on boat dynamics.

This survey on the simulation of platforms propelled by wing sails shows that none utilizes the ROS middleware and the Gazebo simulator. The work presented in this article offers a novel simulated environment for autonomous land yachts using the ROS middleware and the Gazebo simulator. Furthermore, two Gazebo plugins are developed to (*i*) act as a wind sensor and (*ii*) to set the flap angular position.

This article is a condensed version of the thesis presented in [28] and contributes to robotic sailing through the design, modelling and simulation of an autonomous rigid wing sail land yacht, which can be used to survey and monitor the shoreline (more specifically sandy areas), with the help of the Gazebo[1] simulator and the Robot Operating System (ROS)[2] middleware. Moreover, the proposed method can be followed to perform *a priori* evaluation of alternative wing configurations and control algorithms, *i.e.*, without the need to build the actual land yachts. The proposed method constitutes a novel approach to the design and simulation of free rotating wing sail autonomous land yachts. This kind of sail, which is is controlled trough the tail flap, minimises the energy consumed by the sail control system. Once actuated, the flap generates a linear force that induces torque on the wing sail. This shifts slightly the wing sail from the wind direction, defining the sail's angle of attack.

2. Materials and Methods

This work applies the principles of land sailing physics to the design, modelling and simulation of a shore monitoring land yacht. The next subsections cover these different stages, detailing the relevant steps required to reproduce the results.

A rigid-wing sail land yacht uses an airfoil as a sail instead of a conventional cloth sail [12]. The wing sail generates aerodynamic forces, such as lift and drag, and is more efficient, robust and easier to control than conventional cloth sails as, generally, these cloth sails require more than one actuator to be controlled and a wing sail only requires one [12]. Even though wind propelled vehicles, when compared with their fuel or electricity based counterparts, display greater power autonomy, it can be further increased with the adoption of a free rotating wing sail equipped with a wing flap. By default, a free rotating wing sail automatically aligns to the wind direction, defining an angle between the cord of the wing and the oncoming wind flow, called angle of attack. This angle of attack can be controlled by changing the direction of the wing flap. Specifically, when the angle between the wing flap and the apparent wind changes, it generates a linear force that induces torque on the wing sail, defining a new angle of attack.

2.1. Platform Design

The proposed land yacht has a four wheeled chassis, similar to the prototypes presented in [11,15,17]. The chassis, made of stainless steel grade 316L with a density of 7990 kg/m^3, has a parallelepipedic shape with a width of 360 mm, a length of 700 mm and a thickness of 5 mm, totalling 10 kg. Together, the wing, flap and mast weigh 6 kg. The wing and flap airfoils share the same symmetrical National Advisory Committee for Aeronautics (NACA) profile. The expected maximum payload of the land yacht is 4 kg.

The land yacht determines its current state with the help of a set of sensors: (*i*) a GNSS receiver for the position, an inertial sensor for the attitude, an absolute rotary encoder for the wing sail direction; (*ii*) a wind sensor for the apparent wind direction; and (*iii*) from the previous sensor information, the angle of attack of the wing sail. Given a mission, the land yacht calculates the desired heading angle (yacht) and angle of attack (wing sail) to go to the next way point and actuates two servo motors to control the wing flap and the steering mechanism accordingly. The concept of the designed land yacht is shown in Figure 1a.

[1] Gazebo simulator website: http://gazebosim.org
[2] ROS website: https://www.ros.org

(a) Concept **(b)** NACA63(3)-018 2D profile

Figure 1. Land Yacht Design

2.2. Wing Sail Design

The method adopted to define the physical characteristics of the wing sail was suggested by [29]. The angle of attack α of a wing sail corresponds to the angle between the wing chord and the apparent wind direction. Non-null α values generate perpendicular and parallel forces relative to the apparent wind, known as lift (L) and drag (D), and their magnitude depends on the corresponding lift (C_L) and drag (C_D) coefficients [30].

The selected wing profile was a NACA63(3)-018 symmetrical airfoil as it provides a high lift to drag ratio (73) for an $\alpha = 6.75°$ as well as keeps a low drag coefficient (0.02) at $\alpha = 10°$, with a Reynolds number of 500 000 [31,32]. The 2D profile of the NACA63(3)-018 airfoil is presented in Figure 1b.

The lift and drag forces produced in a sail depend on its shape and dimensions. In this case, the area of the wing sail surface needs to generate sufficient lifting force to move the land yacht. The lift force is presented in Equation (1), where ρ is the air density, V is the apparent wind velocity, A is the airfoil lateral area (chord $\times$ wingspan) and C_L is the airfoil lift coefficient.

$$L = \frac{1}{2}\rho V^2 A C_L \tag{1}$$

The drag force is given by Equation (2), where ρ is the air density, V is the apparent wind velocity, A is the airfoil lateral area (chord $\times$ wingspan) and C_D is the airfoil drag coefficient.

$$D = \frac{1}{2}\rho V^2 A C_D \tag{2}$$

Figure 2 displays the lift L and drag D components of the generated aerodynamic force R, the angle between the vehicle's heading and the apparent wind θ, the wing sail angle of attack α, and the driving or thrust T force and lateral or heel H force applied to the vehicle. The force required to put the land yacht in motion is given by Newton's second law presented in Equation (3), where m and a are the land yacht mass and acceleration, respectively. In this case, the mass of the vehicle, comprising the chassis, wing set and maximum payload, is assumed to be 20.0 kg.

$$F = ma \tag{3}$$

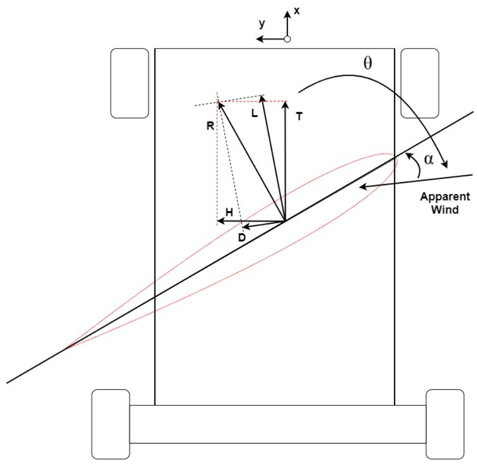

Figure 2. Land Yacht Forces

Replacing the force with the lift expression presented in Equation (1) and adding the friction force, results Equation (4), where μ is the friction coefficient and g is the gravitation acceleration.

$$\frac{1}{2}\rho V^2 A C_L = ma + \mu mg \tag{4}$$

Given that the lift force is perpendicular to the apparent wind direction and the drag force is parallel to the apparent wind direction, the thrust force required to move the land yacht forward T, which is parallel to the vehicle's x axis, is related to the lift and drag through θ, the angle of the apparent wind. This thrust force can, then, be expressed by Equation (5).

$$T = Lsin\theta - Dcos\theta \tag{5}$$

From the combination of Equations (4) and (5) results Equation (6), which represents the equilibrium of forces involved in the forward motion of the land yacht.

$$\frac{1}{2}\rho V^2 A C_L (Lsin\theta - Dcos\theta) = ma + \mu mg \tag{6}$$

Identically, the lateral or heel force applied to the vehicle's y axis is expressed by Equation (7), where θ represents the apparent wind angle.

$$H = Lcos\theta + Dsin\theta \tag{7}$$

Assuming that: (*i*) the land yacht has a mass of 20.0 kg, an initial acceleration of 0.15 m/s^2 (to start moving), and a rolling friction coefficient of 0.002 (bicycle tires on dry concrete[3]); (*ii*) the apparent wind has a velocity of 5 m/s, an angle $\theta \leq 45^o$ and the air density is 1.225 kg/m^3; and (*ii*) the NACA63(3)-018 symmetrical airfoil profile has a lift coefficient of 0.75 with α = 10° [31], the wing area given by Equation (6) is approximately 0.4 m^2. Based on this set of assumptions, the NACA63(3)-01 wing sail has a chord of 400 mm and a wingspan of 1000 mm, whereas the NACA63(3)-01 flap presents a chord of 130 mm and a wingspan of 330 mm.

To determine if the stability of the vehicle, it is necessary to consider the existing rolling and anti-rolling moments. According to [12], the rolling moment M_r generated by the lateral wind on the wing sail is given by Equation (8), where L_e is the wing sail wingspan, Δh is the wing sail mounting

3 http://physicalcycling.com/tire-traction

distance, P_r is the true atmospheric pressure, P_s is the mass-specific gas constant and T_r is the air temperature.

$$M_r = \frac{88.296 P_r V^2 A(C_L cos(\theta) + C_D sin(\theta))[L_e^2 - 100^2 + 2\Delta h(L_e - 100)]}{(273.15 + T_r) P_s L_e} \tag{8}$$

The anti-rolling moment moment M_a, generated by the vehicle as a whole, is given by Equation (9) [12], where B_1 and B_2 are the front and rear wheel base lines, respectively.

$$M_a = mg(B_1 + B_2)/4 \tag{9}$$

The critical vehicle tipping wind velocity occurs with lateral apparent wind, *i.e.*, $\theta = 90°$ and $\alpha = 90°$. From Equation (8), $\theta = 90°$, $C_L = 0$ (value of C_L for $\alpha = 90°$ [31]) and $C_D = 2$ (value of C_D for $\alpha = 90°$ [31]), results Equation (10).

$$V \leq \sqrt{\frac{(273.15 + T_r)(B_1 + B_2) mg L_e P_s}{724.33 A(L_e^2 + 2\Delta h L_e - 100^2 - 200\Delta h) P_r}} \tag{10}$$

Finally, assuming that T_r = 20°C, B_1 = 0.5 m, B_2 = 0.38 m,m = 20 kg, g = 9.81 m/s^2, L_e = 1 m, P_s = 8.31432 × 10^3 N m kmol^{-1} K^{-1}, Δh = 0.1 m and P_r = 101 325 Pa, the maximum wind velocity that the vehicle can withstand is 12 m/s.

2.3. Platform Simulation

The simulation was performed with the Gazebo simulator and the ROS middleware. The Gazebo simulator, which is a three-dimensional open-source dynamics simulator for robotic platforms, was chosen as it allows the definition of new models in Simulation Description Format (SDF), provides a plugin that simulates aerodynamic forces and is ROS compatible. SDF models comprise collections of: (*i*) links, corresponding to body parts and including collision (geometry), visual (visualization) and inertia (dynamics) elements; (*ii*) joints between links, specifying the parent and child relationship, the axis of rotation and limits of the joint; (*iii*) sensors that collect world data for plugins; and (*iv*) plugins which control the behaviour of the model [33].

2.3.1. 3D Model

The vehicle and wing sail model were created using the Fusion 360 Computer-Aided Design software from AutoDesk. The resulting 3D mesh files were imported to Gazebo through the SDF model file, which describes the links and joints of the different parts of the land yacht and loads model related plugins, such as the aerodynamics or the sensor plugins. Listing 1 defines a link and imports the corresponding 3D mesh file into Gazebo. The link element contains the link name, the link pose relative to the base link (in this case the base link is the chassis), the inertial properties (such as mass and the inertial matrix), the link collision properties (in this case the collision zone is the same as the model format) and the link visual format.

Listing 2 specifies a joint between two links, including the joint type (since it is connecting a wheel, then the joint type is revolute), the joint name, the pose relatively to the child link, the child and parent links (in this case it is the wheel and the chassis, respectively), the rotation axis (in this case the joint rotates in the y axis), and the joint friction and damping. Finally, the SDF world file loads the land yacht model file as well as the environmental characteristics, such as the ambient light and ground plane, and the world related plugins. The land yacht model presented in Figure 3 is composed of a chassis, four wheels, a steering mechanism composed of 4 links, a wing sail and a flap (11 links and 12 joints).

Listing 1: SDF Link Example

```xml
<link name='steering_middle'>
    <pose>3.373 -0.12 0.6 0 0 0</pose>
    <inertial>
        <mass>0.195315</mass>
        <inertia>
            <ixx>1.614e-3</ixx>
            <ixy>4.98132e-7</ixy>
            <ixz>1.72258e-7</ixz>
            <iyy>7.383226e-6</iyy>
            <iyz>2.843631e-6</iyz>
            <izz>1.612e-3</izz>
        </inertia>
    </inertial>
    <collision name='collision'>
        <geometry>
            <mesh>
                <uri>model://my_robot/Cad_Files/SteeringMiddleGazebo.stl</uri>
                <scale>0.01 0.01 0.01</scale>
            </mesh>
        </geometry>
    </collision>
    <visual name='visual'>
        <geometry>
            <mesh>
                <uri>model://my_robot/Cad_Files/SteeringMiddleGazebo.stl</uri>
                <scale>0.01 0.01 0.01</scale>
            </mesh>
        </geometry>
    </visual>
</link>
```

Listing 2: SDF Joint Example

```xml
<joint type="revolute" name="left_back_wheel_hinge">
    <pose>0 0 0 0 0 0</pose>
    <child>left_back_wheel</child>
    <parent>chassis</parent>
    <axis>
        <xyz>0 1 0</xyz>
        <dynamics>
            <friction>0.0625</friction>
            <damping>0.4</damping>
        </dynamics>
    </axis>
</joint>
```

2.3.2. ROS Integration

To launch Gazebo using ROS, the package `gazebo_ros_pkgs`[4] was reused. This package enables the interface between ROS and Gazebo, allowing also the creation of ROS nodes inside Gazebo plugins. A ROS package, named `land_yacht`, was created specifically for the development of the simulation. This package uses a launch file to load an empty world from `gazebo_ros_pkgs` together with the

[4] gazebo_ros_pkgs website: http://wiki.ros.org/gazebo_ros_pkgs

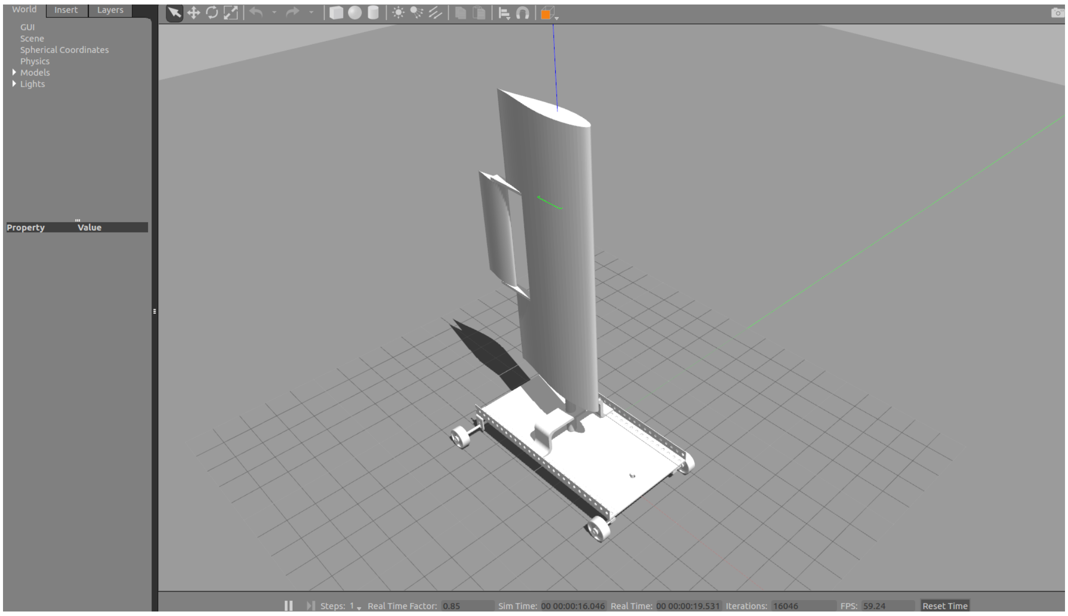

Figure 3. Land Yacht 3D Model in Gazebo

model of the land yacht, and a node responsible for the control of the wing flap and the steering. This empty world serves merely as an interface between `gazebo_ros_pkgs` and `land_yacht`. For this to be possible, the world file, which loads the vehicle model, must be stored in a subfolder of the ROS package named `worlds`. A block diagram of this setup is presented in Figure 4.

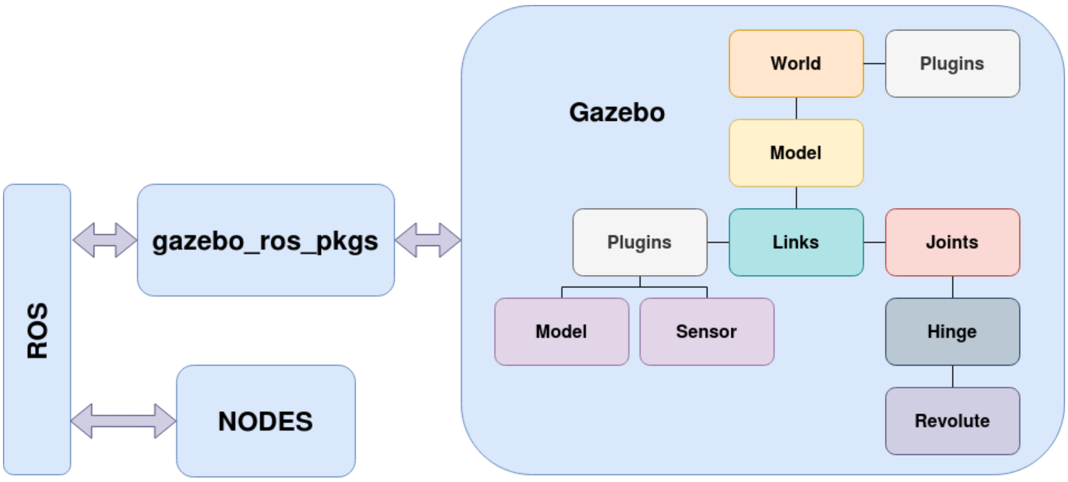

Figure 4. Gazebo-ROS Interface Block Diagram [28]

2.3.3. Gazebo Plugins

The simulation of the land yacht uses three plugins: a modified `liftdragplugin`[5] and two new plugins named `land_yacht_plugin` and `land_yacht_appar_wind`. The `land_yacht_plugin` enables the control from ROS of the wing sail flap and of the land yacht steering; and the `land_yacht_appar_wind` plugin simulates an apparent wind sensor (velocity and direction of the wind relative to the land yacht).

[5] Gazebo aerodynamics plugin: http://gazebosim.org/tutorials?tut=aerodynamics&cat=physics

The `liftdragplugin` simulates the aerodynamic forces and the pitching moment on an airfoil (the torque generated by the wind on the airfoil), since it was developed for airplanes. Given that an airfoil on a land yacht is positioned vertically, the plugin will calculate the yawing moment. In short, the `liftdragplugin`, apart from generating lift and drag forces, also aligns the wing sail to the direction of the wind. However, this plugin was created to simulate these forces on aeroplanes or fixed wing drones in windless conditions. In other words, this plugin assumes the world's wind velocity corresponds to the world's linear velocity of the vehicle, which, in this case, is only partially correct. The plugin was modified to add the world's wind velocity to the world's linear velocity of the vehicle. For example, if the vehicle is moving westward with a linear velocity of 1 m/s and there is a westerly wind of 2 m/s, then the two linear velocities are added, generating a total apparent wind velocity of 3 m/s. Without this change, the apparent wind velocity would remain 1 m/s. Finally, the plugin was also adapted to subscribe a ROS topic that broadcasts the world's wind velocity in the x and y axis. Figure 5 displays a diagram that details the processing pipeline of the modified plugin. Before calculating the lift and drag forces, the plugin subtracts the vehicle linear velocity and the true wind velocity in the world frame and, subsequently, uses the vehicle orientation to establish the apparent wind, which corresponds to the relative wind to the vehicle. With the apparent wind and the wing sail angular position, the plugin calculates the wing sail angle of attack (AoA) and, using the linearised airfoil parameters, determines the lift and drag coefficients. With these coefficients, the plugin calculates the lift and drag forces to get the resulting force. This resulting force is applied to the wing sail pressure point, in this case it is situated in the middle of the wing, and is also used to calculate its yawing moment. This yawing moment is translated into torque and, finally, applied to the wing sail.

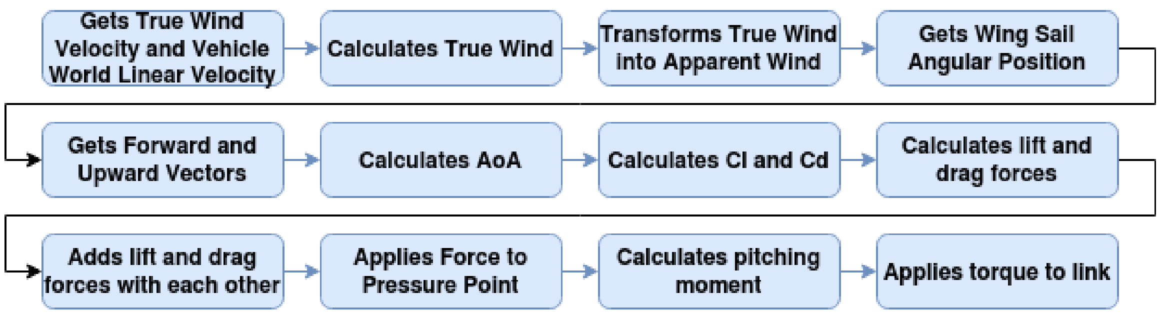

Figure 5. Liftdragplugin Diagram

The `land_yacht_plugin` is composed of a ROS node that subscribes two topics – the flap angle and steering angle – and publishes the vehicle ground truth for control and debugging. When the plugin receives new messages from the subscribed topics it sets the corresponding joint angle to the broadcasted value.

The `land_yacht_appar_wind` plugin converts the true wind (velocity and direction in the world reference frame) into the vehicle's apparent wind (velocity and direction in the vehicle reference frame). It subscribes the true wind topic, transforms the true into the apparent the wind, using the vehicle's heading and velocity in the world reference frame, and, finally, publishes the result in a new topic.

Plugins can be loaded in the model or the world SDF file. Listing 3 illustrates the loading of the `liftdragplugin`. The NACA63(3)-018 airfoil characteristics correspond to the stall and the slopes of the lines obtained from linearising the characteristic lift and drag coefficient curves [31], shown in the example presented in Figure 6. Each curve is approximated by two lines which intersect at the stall of the curve and these line slopes are used to describe the airfoil.

2.3.4. Wing Sail Control

The control of the angle of attack of the wing sail is indirect, *i.e.*, it is set through the flap. The flap has a Proportional-Differential (PD) controller which uses as inputs the apparent wind direction

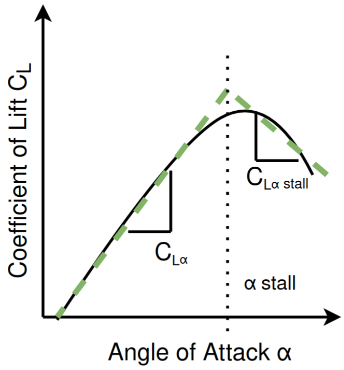

Figure 6. Liftdragplugin Curve Linearization Example

Listing 3: SDF Plugin Example

```
<plugin name="sail_plugin" filename="libTese_LiftDragPlugin.so">
  <a0>0.0</a0>
  <cla>5.72957795131</cla>
  <cda>-0.57295779513</cda>
  <cma>-0.05</cma>
  <alpha_stall>0.17453292519</alpha_stall>
  <cla_stall>-2.86478897565</cla_stall>
  <cda_stall>2.29183118052</cda_stall>
  <cma_stall>0.2 </cma_stall>
  <cp>0.05 0 1.5</cp>
  <area>0.4</area>
  <fluid_density>1.2041</fluid_density>
  <forward>-1 0 0</forward>
  <upward>0 1 0</upward>
  <link_name>wing_sail</link_name>
  <radial_symmetry>true</radial_symmetry>
</plugin>
```

(published in the apparent wind topic) and the wing sail angular position (published in the sail rotation topic), and outputs the desired flap angle. A block diagram of the wing flap control is presented in Figure 7, where e is the error and de the differential error between the desired and the current angle of attack, and K_p and K_d are the proportional and differential gains, respectively.

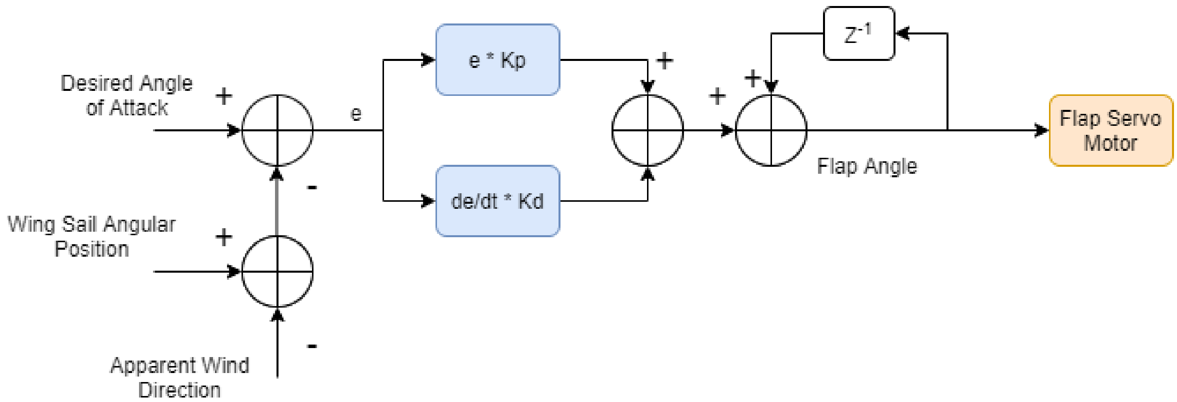

Figure 7. Flap Control Block Diagram

3. Results & Discussion

3.1. Experimental Setup

Figure 8 presents the set of nodes and topics involved in this experimental setup. The Gazebo environment (`gazebo` node) subscribes the wind, steering and flap topics and publishes the ground truth as well as the sail rotation and apparent wind topics. The control node (`land_yacht_control`) subscribes the ground truth, the sail rotation and the apparent wind from Gazebo, and publishes the flap control topics. The `true_wind_generator` node generates and publishes the real time true wind conditions (in the world reference frame). The `teleop_key_pub` manual control node reuses the `teleop_twist_keyboard`[6] package and was added to the setup for debugging purposes.

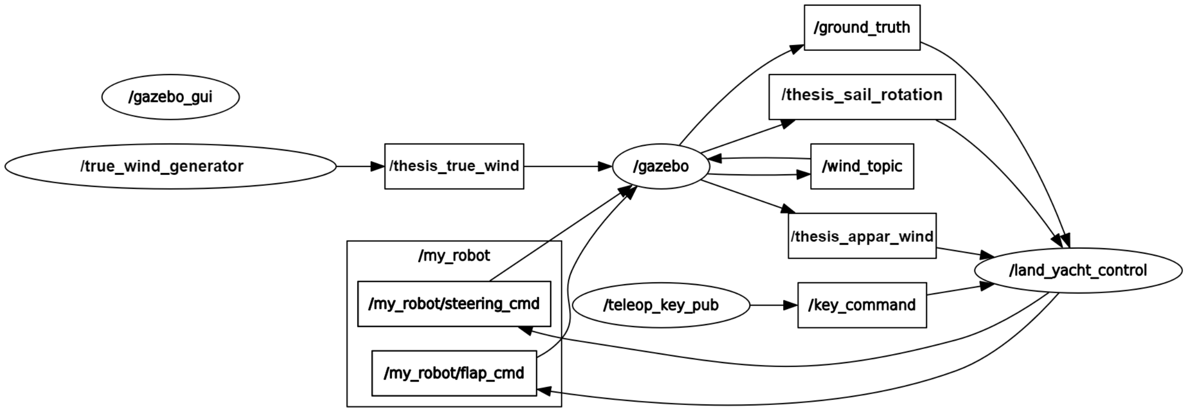

Figure 8. Experimental Setup

3.2. Wing Sail Alignment to the Wind

This test validates the wing sail alignment to the wind without any control on the flap (the flap remains aligned with the wing sail at all times). The behaviour of the wing sail was tested with an initial apparent wind direction of 90° ($\alpha_i = 90°$) and apparent wind velocities of 8 kn, 9 kn and 10 kn. The final desired angle of attack is 0° ($\alpha_f = 0°$). The wing sail response is presented in Figure 9, where the blue arrow is the wind direction and the dashed red line is the wing sail direction.

Figure 10 displays the time response of the wing sail angle of attack. These results show that, when the wing and tail are aligned, the wing sail aligns automatically to the wind due to the yawing moment of the aerodynamics plugin. Although the wing sail takes identical time to stabilise with different wind velocities, the higher the wind velocity, the higher the overshoot.

3.3. Wing Sail Response to the Flap Angle

These tests verify if the wing sail turns correctly given a change in the flap angle. Initially, the wing sail was aligned to the apparent wind direction ($\alpha_i = 0°$) and the flap angle was set to 0°. The test consisted of turning the flap manually, using the keyboard, to the left and to the right, as is presented in Figure 11. The wing sail responded correctly to the flap angle change. It turned to the right when the flap angle was set to the left, and to the left when the flap angle was set to the right.

---

6 teleop_key_pub website: http://wiki.ros.org/teleop_twist_keyboard

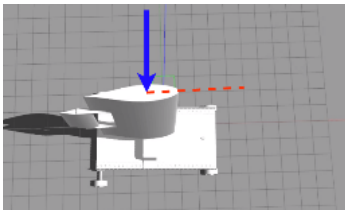

(a) $t = 0$ s

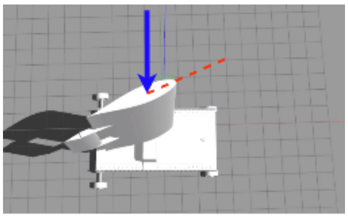

(b) $t = 1$ s

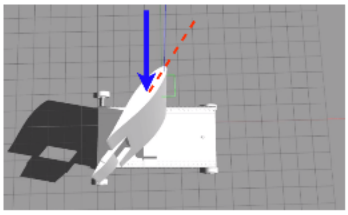

(c) $t = 2$ s

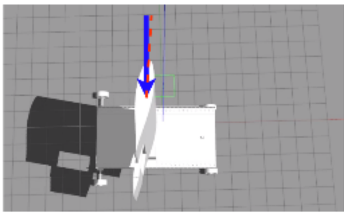

(d) $t = 3$ s

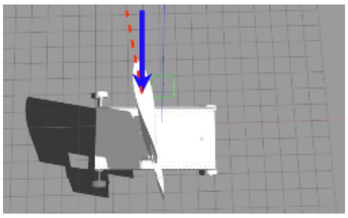

(e) $t = 4$ s

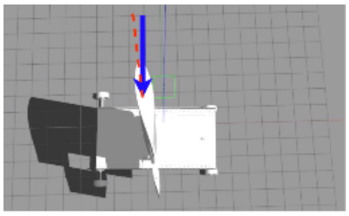

(f) $t = 5$ s

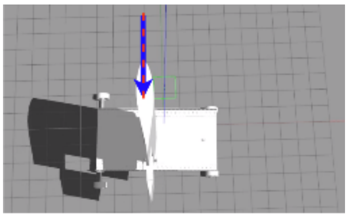

(g) $t = 6$ s

Figure 9. Wing Sail Alignment to the Wind Over Time (10 kn)

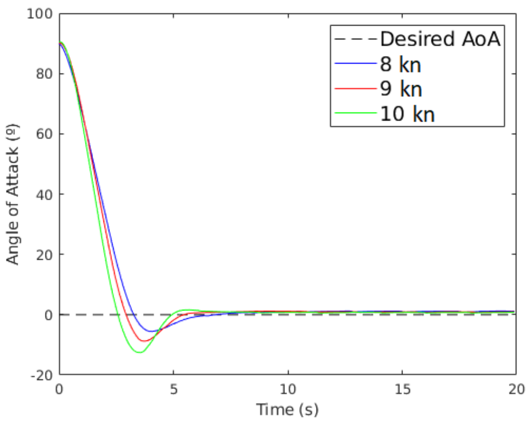

Figure 10. Time Response of the Wing Sail AoA ($\alpha_i = 90°$, $\alpha_f = 0°$)

3.4. Setting the Wing Sail to an Angle of Attack

These tests check if the wing sail direction is controllable through the flap angle. Specifically, it verifies if the wing sail stabilizes at a defined angle of attack. The apparent wind direction was set to 90° ($\alpha_i = 90°$), the apparent wind velocity to 8 kn, 9 kn and 10 kn, and the final desired angle of attack (α_f) to 10°. Figure 12 plots the obtained time responses. The wing sail direction overshoots the desired angle of attack but stabilizes after a few seconds. These results validate the wing sail control as it successfully stabilized the wing sail to the defined angle of attack.

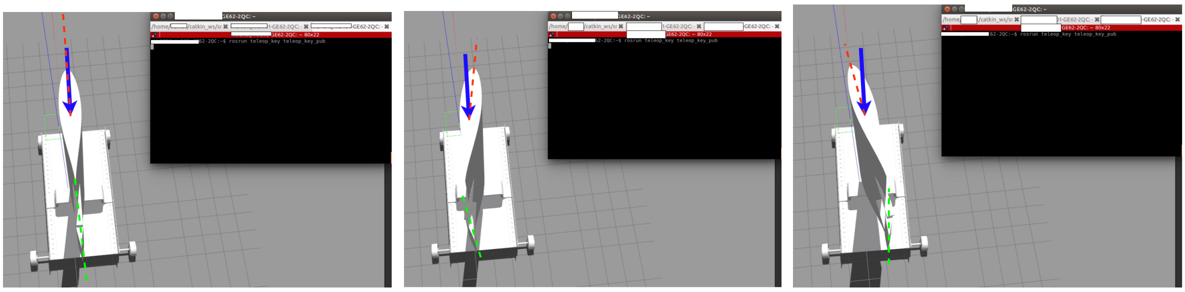

(a) Flap and Wing Aligned **(b)** Flap Turned Right **(c)** Flap Turned Left

Figure 11. Wing Sail Response to Flap Angle Changes (8 kn)

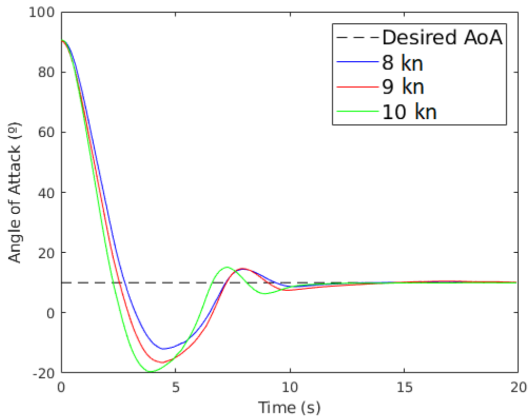

Figure 12. Time Response of the Wing Sail AoA ($K_p = 0.05$, $K_d = 0.07$, $\alpha_i = 90°$, $\alpha_f = 10°$)

3.5. Vehicle Motion

The final experiment tests if the wing sail provides enough lift to displace the vehicle. The initial apparent wind direction was set to 90° ($\alpha_i = 90°$), the apparent wind velocity to 8 kn, 9 kn and 10 kn, and the final desired angle of attack (α_f) to 10°. Figure 13 shows the vehicle velocity over time. Initially,

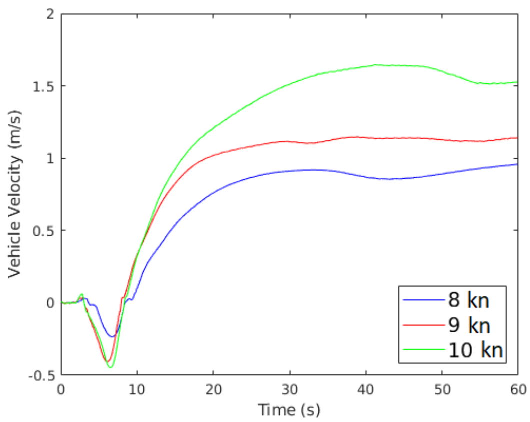

Figure 13. Vehicle Velocity Over Time ($K_p = 0.05$, $K_d = 0.07$, $\alpha_i = 90°$, $\alpha_f = 10°$)

the vehicle displays negative velocities because the wing sail overshoots the desired angle of attack for a short period of time. With negative angle of attack values, negative lift coefficients are obtained and, consequently, negative accelerations, making the vehicle move slightly backwards. After this period, the vehicle starts moving forward with positive acceleration. The velocity increases until the acceleration of the vehicle becomes null or the terminal maximum velocity is achieved. The velocity can be reduced by changing the angle of attack of the wing sail until, ultimately, it becomes zero, eventually stopping the vehicle. This experiment shows that the wing sail was able to provide enough lift to move the vehicle.

3.6. Polar Diagram

The polar diagram characterises the optimal performance of a wind propelled platform as a function of the wind velocity and apparent wind angle. In this test, the autonomous flap control was responsible for the optimisation of the lift force applied to the wing sail. Three different wind velocities were simulated (8 kn, 9 kn and 10 kn) together with apparent wind direction increments of 5° from 0° to ±180°.

The velocity started increasing at approximately ±45° until peaked at ±90°. After peaking, the maximum velocity started decreasing until it reached null values near ±180°, as shown in the polar diagram presented in Figure 14. The no go zone is visible between −45° and 45°, and between −135° and 135°.

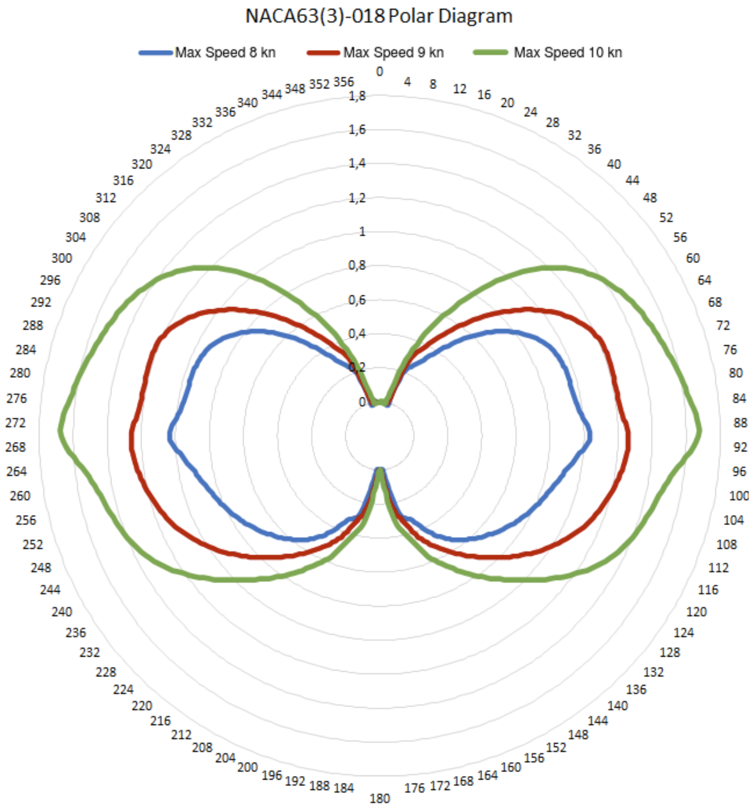

Figure 14. Land Yacht Polar Diagram

4. Conclusions

The design, modelling and simulation of an autonomous wing sail land yacht was successful as the wing sail responded correctly to the wind direction and to changes in the flap angle. Furthermore, the sailing behaviour of the designed land yacht is characterised by its polar diagram. Some of the values used in the modelling and simulation were arbitrated since there was no possibility of obtaining them through experimentation. This simulated environment can be further enhanced to provide several different scenarios, such as sandy coastal regions, and can be utilised by a different modelled land yacht with a different type of airfoil, provided the airfoil characteristics. Although the control was not the main focus of this work, it can also be refined to solve the identified frailties. Future work will focus on experimenting with different types of airfoils and control techniques.

Author Contributions: Vítor Tinoco was responsible for the investigation, implementation of the methodology and software as well as the preparation of the original draft. Benedita Malheiro and Manuel F. Silva contributed with the conceptualization, review and editing, supervision and funding acquisition.

Funding: This work was partially financed by National Funds through the FCT – Fundação para a Ciência e a Tecnologia (Portuguese Foundation for Science and Technology) as part of project UIDB/50014/2020.

Conflicts of Interest: The authors declare no conflict of interest.

Abbreviations

The following abbreviations are used in this manuscript:

α	Angle of Attack
α_i	Initial Angle of Attack
α_f	Final Angle of Attack
θ	Angle of the Apparent Wind
AoA	Angle of Attack
GNSS	Global Navigation Satellite System
NACA	National Advisory Committee for Aeronautics
PD	Proportional-Differential
ROS	Robot Operating System
SDF	Simulation Description Format

References

1. National Academy of Engineering. *Autonomy on Land and Sea and in the Air and Space: Proceedings of a Forum*; The National Academies Press: Washington, DC, 2018. doi:10.17226/25168.
2. Zhu, X.; Kim, Y.; Minor, M.A.; Qiu, C. *Autonomous Mobile Robots in Unknown Outdoor Environments*; CRC Press: Boca Raton, FL, USA, 2020.
3. Springer, P.J. *Outsourcing War to Machines – The Military Robotics Revolution*; Praeger Security International: Santa Barbara, California, 2018.
4. Kimball, J. *Physics of Sailing*; CRC Press, 2009.
5. Miller, P.H.; Hamlet, M.; Rossman, J. Continuous Improvements to USNA SailBots for Inshore Racing and Offshore Voyaging. Robotic Sailing 2012 – Proceedings of the 5th International Robotic Sailing Conference, 2012, pp. 49–60. doi:10.1007/978-3-642-33084-1_5.
6. Anthierens, C.; Pauly, E.; Jeay, F. MARIUS: A Sailbot for Sea-Sailing. Robotic Sailing 2013 – Proceedings of the 6th International Robotic Sailing Conference, 2013, pp. 3–12. doi:10.1007/978-3-319-02276-5_1.
7. Miller, P.; Sauzé, C.; Neal, M. Development of ARRTOO: A Long-Endurance, Hybrid-Powered, Oceanographic Research Vessel. Robotic Sailing 2013 – Proceedings of the 6th International Robotic Sailing Conference, 2013, pp. 53–65. doi:10.1007/978-3-319-02276-5_5.
8. Silva, M.F.; Friebe, A.; Malheiro, B.; Guedes, P.; Ferreira, P.; Waller, M. Rigid wing sailboats: A state of the art survey. *Ocean Engineering* **2019**, *187*, 106–150.
9. Shukla, P.C.; Ghosh, K. Revival of the Modern Wing Sails for the Propulsion of Commercial Ships. *International Journal of Physical and Mathematical Sciences* **2009**, *3*, 207 – 212.
10. Landis, G.; et al.. NIAC Phase 1 Final Report: Venus Landsailer Zephyr. Technical report, NASA, 2014.
11. Xie, S.; Chen, J.; li, H.; Luo, J.; Pu, H.; Peng, Y. The research on wing sail of a land-yacht robot. *Advances in Mechanical Engineering* **2015**, *7*, 1–19. doi:10.1177/1687814015623144.
12. Xie, S.; Feng, K.; Peng, Y.; Luo, J.; Chen, J.; Gu, J. Design and analysis of an autonomous controlled four wheeled land yacht. *2014 IEEE International Conference on Information and Automation, ICIA 2014* **2014**, pp. 773–778. doi:10.1109/ICInfA.2014.6932756.
13. Zhu, A.; Beer, C.; Juhandi, K.; Orlov, M.; Bacau, N.; Kádár, L.; Duarte, A.J.; Malheiro, B.; Justo, J.; Silva, M.F.; Ribeiro, M.C.; Ferreira, P.D.; Guedes, P. Sail Car – An EPS©ISEP 2019 Project. 2020 IEEE Global Engineering Education Conference (EDUCON), 2020, pp. 487–492. doi:10.1109/EDUCON45650.2020.9125314.
14. Landis, G.A.; Oleson, S.R.; Grantier, D. Zephyr: A Landsailing Rover for Venus. 65th International Astronautical Congress, 2014, p. 14.

15. Chen, J.; Ye, Z.; Yang, R.; Cai, G.; Li, J.; Li, H. Design and Control of Multiple Wing-sail Land Yacht Robot. 2018 IEEE International Conference on Mechatronics and Automation (ICMA), 2018, pp. 1800–1805. doi:10.1109/ICMA.2018.8484725.
16. Mirzaei, P.A.; Rad, M. Toward design and fabrication of wind-driven vehicles: Procedure to optimize the threshold of driving forces. *Applied Mathematical Modelling* **2013**, *37*, 50 – 61. doi:10.1016/j.apm.2011.11.037.
17. Dong, Y.; Ding, X.; Li, Z.; Zhang, L.; Liu, H.; Ding, N.; Sun, Z.; Qian, H. Wing Sail Land-yacht Modeling And System Verification. 2019 IEEE International Conference on Robotics and Biomimetics (ROBIO), 2019, pp. 1350–1355. doi:10.1109/ROBIO49542.2019.8961489.
18. Reina, G.; Foglia, M. Modelling and handling dynamics of a wind-driven vehicle. *Vehicle System Dynamics* **2019**, *57*, 697–720. doi:10.1080/00423114.2018.1479529.
19. Eliasson, R.; Larsson, L.; Orych, M. *Principles of Yacht Design*; Bloomsbury Publishing, 2014.
20. Elkaim, G. Autonomous Surface Vehicle Free-Rotating Wingsail Section Design and Configuration Analysis. *Journal of Aircraft - J AIRCRAFT* **2008**, *45*, 1835–1852. doi:10.2514/1.27284.
21. Neal, M. A Hardware Proof of Concept of a Sailing Robot for Ocean Observation. *IEEE Journal of Oceanic Engineering* **2006**, *31*, 462–469. doi:10.1109/JOE.2006.875101.
22. Friebe, A.; Olsson, M.; Le Gallic, M.; Springett, J.L.; Dahl, K.; Waller, M. A marine research ASV utilizing wind and solar power. OCEANS 2017 - Aberdeen, 2017, pp. 1–7. doi:10.1109/OCEANSE.2017.8084648.
23. Chen, J.; Xie, S.; Luo, J.; Li, H. Wind-driven land-yacht robot mathematical modeling and verification. *Ind. Robot* **2016**, *43*, 77–90.
24. Rynne, P.F.; von Ellenrieder, K.D. Development and Preliminary Experimental Validation of a Wind- and Solar-Powered Autonomous Surface Vehicle. *IEEE Journal of Oceanic Engineering* **2010**, *35*, 971–983. doi:10.1109/JOE.2010.2078311.
25. Enqvist, T.; Friebe, A.; Haug, F. Free Rotating Wingsail Arrangement for Åland Sailing Robots. Robotic Sailing 2016; Alves, J.C.; Cruz, N.A., Eds.; Springer International Publishing: Cham, 2017; pp. 3–18. doi:10.1007/978-3-319-45453-5_1.
26. Augenstein, T.; Singh, A.; Miller, J.; Pomerenk, A.; Dean, A.; Ruina, A. Using a Controlled Sail and Tail to Steer an Autonomous Sailboat. Robotic Sailing 2016; Alves, J.C.; Cruz, N.A., Eds.; Springer International Publishing: Cham, 2017; pp. 91–103. doi:10.1007/978-3-319-45453-5_8.
27. Setiawan, J.D.; Chrismianto, D.; Ariyanto, M.; Sportyawan, C.W.; Widyantara, R.D.; Alimi, S. Development of Dynamic Model of Autonomous Sailboat for Simulation and Control. 2020 7th International Conference on Information Technology, Computer, and Electrical Engineering (ICITACEE), 2020, pp. 52–57. doi:10.1109/ICITACEE50144.2020.9239150.
28. Tinoco, V. Modelling and Simulation of a Wing Sail Land Yacht. Master's thesis, School of Engineering, Polytechnic of Porto, Porto, Portugal, 2020.
29. Silva, M.F.; Malheiro, B.; Guedes, P.; Ferreira, P. Airfoil Selection and Wingsail Design for an Autonomous Sailboat. Robot 2019: Fourth Iberian Robotics Conference; Silva, M.F.; Lima, J.L.; Reis, L.P.; Sanfeliu, A.; Tardioli, D., Eds.; Springer International Publishing: Cham, 2020; pp. 305–316. doi:10.1007/978-3-030-35990-4_25.
30. Getzan, G.D.; Shimada, M.; Shimoyama, I.; Matsumoto, Y.; Miura, H. Aerodynamic behavior of microstructures. ETFA '94. 1994 IEEE Symposium on Emerging Technologies and Factory Automation. (SEIKEN) Symposium - Novel Disciplines for the Next Century- Proceedings, 1994, pp. 54–61. doi:10.1109/ETFA.1994.402023.
31. Airfoil Tools. NACA 63(3)-018 (naca633018-il). http://airfoiltools.com/airfoil/details?airfoil=naca633018-il, 2020. Last accessed 28 November 2020.
32. Drela, M. XFOIL: An Analysis and Design System for Low Reynolds Number Airfoils. Low Reynolds Number Aerodynamics; Mueller, T.J., Ed.; Springer Berlin Heidelberg: Berlin, Heidelberg, 1989; pp. 1–12.
33. Rivera, Z.B.; Simone, M.C.D.; Guida, D. Unmanned Ground Vehicle Modelling in Gazebo/ROS-Based Environment. *Machines* **2019**, *7*, 42. doi:10.3390/machines7020042.

Sample Availability: https://1drv.ms/u/s!Amsuyvsv73czu1bUoPfhiI2n2NZK?e=JYIcfv